JACS
JOURNAL OF THE AMERICAN CHEMICAL SOCIETY
pubs.acs.org/JACS
Article

The Conformational Equilibria of a Human GPCR Compared between Lipid Vesicles and Aqueous Solutions by Integrative ^{19}F-NMR

Arka Prabha Ray,[#] Beining Jin,[#] and Matthew T. Eddy*

Cite This: J. Am. Chem. Soc. 2025, 147, 17612−17625
Read Online

ABSTRACT: Endogenous phospholipids influence the conformational equilibria of G protein-coupled receptors, regulating their ability to bind drugs and form signaling complexes. However, most studies of GPCR−lipid interactions have been carried out in mixed micelles or lipid nanodiscs. Though useful, these membrane mimetics do not fully replicate the physical properties of native cellular membranes associated with large assemblies of lipids. We investigated the conformational equilibria of the human A_{2A} adenosine receptor (A_{2A}AR) in phospholipid vesicles using ^{19}F solid-state magic angle spinning NMR (SSNMR). By applying an optimized sample preparation workflow and experimental conditions, we were able to obtain ^{19}F-SSNMR spectra for both antagonist- and agonist-bound complexes with sensitivity and line widths closely comparable to those achieved using solution NMR. This facilitated a direct comparison of the A_{2A}AR conformational equilibria across detergent micelle, lipid nanodisc, and lipid vesicle preparations. While antagonist-bound A_{2A}AR showed similar conformational equilibria across all membrane and membrane mimetic systems, the conformational equilibria of agonist-bound A_{2A}AR exhibited differences among different environments. This suggests that the conformational equilibria of GPCRs may be influenced not only by specific receptor-lipid interactions but also by the membrane properties found in larger lipid assemblies.

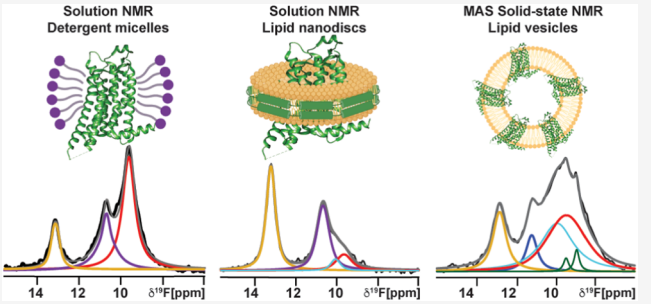

INTRODUCTION

Phospholipids are important endogenous allosteric modulators of G protein-coupled receptors (GPCRs), sensory integral membrane proteins that are essential for most physiological processes. As key components of biological membranes, phospholipids, along with cholesterol, have been frequently observed in close association with GPCRs in cryo-electron microscopy structures of GPCR signaling complexes.[1−6] These structural observations have been bolstered by biophysical approaches, providing insights into the functional importance of GPCR-lipid interactions.[7−11] NMR spectroscopic studies, in particular, have shown that lipids not only associate with GPCRs but also influence the conformational equilibria underpinning the GPCR function, thereby modulating receptor activity in a manner that is highly dependent on the membrane environment.[12−17]

GPCR structures determined by cryo-EM,[18,19] as well as many biophysical experiments studying GPCR-lipid interactions,[20−22] have been studied using either mixed micelles containing detergents and lipids or within lipid nanodiscs, membrane mimetics formed by a scaffold protein surrounding clusters of lipids.[23,24] Although nanodiscs have proven to be valuable biochemical tools, offering a more native-like alternative to detergents for solubilizing GPCRs, they still fall short of fully replicating the properties of biological membranes present in the cellular environment.[25] For example, the ability to alter membrane curvature, recognized for its role in regulating GPCR sorting,[26] is highly restricted in nanodiscs. Additionally, comparisons of lipid phase behavior have observed differences in the phase transitions of lipids between nanodiscs or membranes,[27−31] indicating that properties observed for larger assemblies of lipids are not replicated in nanodiscs. A comparison of cryo-EM structures of an ion channel among differently sized nanodiscs revealed that the size of the lipid nanodisc influenced the determined structure,[32] potentially pointing toward the influence of the scaffolding protein on the properties of the enclosed lipids.

As an alternative to lipid nanodiscs, phospholipid vesicles exhibit properties such as coordinated lipid phase behavior and lipid composition that can be tailored to more accurately represent the same collective lipid properties found in native cellular membranes.[33] We leveraged this strength to investigate

Received: October 27, 2024
Revised: April 30, 2025
Accepted: May 2, 2025
Published: May 16, 2025

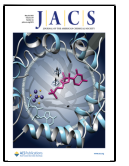

https://doi.org/10.1021/jacs.4c15106
J. Am. Chem. Soc. 2025, 147, 17612−17625

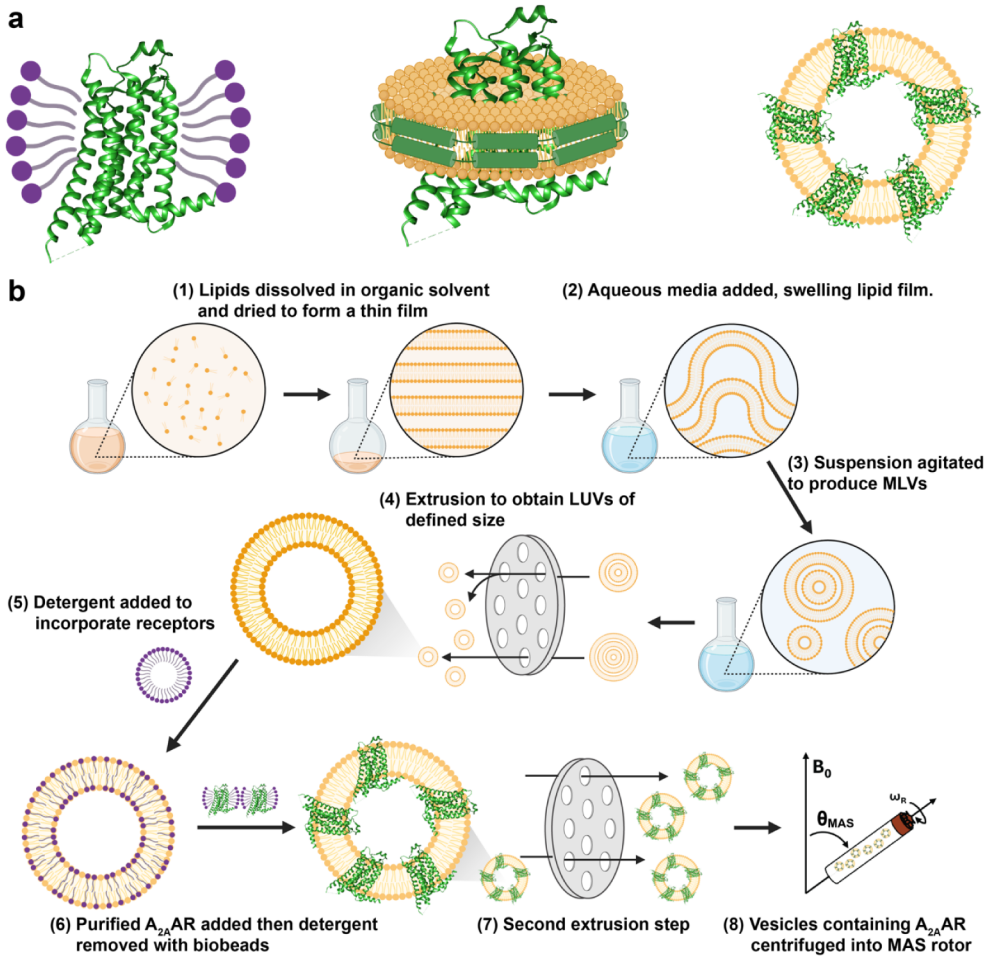

Figure 1. Human $A_{2A}AR$ in different membrane or membrane-mimetic environments and the sample preparation workflow. (a) $A_{2A}AR$ compared in three different environments in this study: (left) detergent micelles, (middle) lipid nanodiscs, and (right) lipid vesicles. (b) Schematic of the sample preparation workflow for preparing lipid vesicles containing ^{19}F-labeled human $A_{2A}AR$ for solid-state MAS NMR experiments.

the conformational equilibria of the human A_{2A} adenosine receptor ($A_{2A}AR$), a representative class A GPCR that has served as an important tool for GPCR biophysical studies,[34−37] in lipid vesicles using ^{19}F magic angle spinning (MAS) solid-state NMR spectroscopy. ^{19}F-NMR offers a unique advantage in solid-state MAS experiments due to its high sensitivity and minimal to no nonspecific background signals, as documented in applications with integral membrane proteins,[38,39] membrane-associated proteins,[40−43] and protein assemblies.[44,45] To facilitate this investigation, we developed a workflow for producing lipid vesicles containing $A_{2A}AR$ for ^{19}F MAS NMR experiments. We confirmed that $A_{2A}AR$ in lipid vesicles maintained the same ligand-binding affinities for antagonists and agonists as $A_{2A}AR$ in mammalian cells, and we confirmed that $A_{2A}AR$ was globally folded in our vesicle preparations. A distinct advantage of $A_{2A}AR$ prepared in lipid vesicles was enhanced thermal stability over $A_{2A}AR$ in either detergent micelles or lipid nanodiscs. By applying optimal sample preparation and experimental NMR conditions, we recorded ^{19}F MAS SSNMR spectra of $A_{2A}AR$ with sensitivity and line widths closely comparable to those observed for $A_{2A}AR$ in aqueous solutions. This enabled a direct comparison of the $A_{2A}AR$ conformational equilibria across lipid vesicles, lipid nanodiscs, and detergent micelle environments. While antagonist-bound $A_{2A}AR$ shared similar conformational equilibria across different environments, we observed differences in the populations of different conformations for agonist-bound $A_{2A}AR$, suggesting that the bulk properties of lipids can affect the conformational landscape of GPCRs.

RESULTS

Reconstitution and Pharmacological Characterization of Functional Human $A_{2A}AR$ in Lipid Vesicles. For all biochemical and NMR experiments, a variant of human $A_{2A}AR$ was utilized containing a single, solvent-accessible cysteine located at position 289 at the intracellular surface of transmembrane (TM) helix VII, $A_{2A}AR$[A289C]. A ^{19}F-2,2,2-trifluoroethanethiol probe was introduced at this position via thiol Michael addition using an in-membrane chemical modification protocol, as described previously.[46] The chemical shift of the ^{19}F-NMR probe located at position 289 was shown to be sensitive to ring current effects from nearby aromatic residues F286$^{7.51}$, F295$^{8.50}$, and F299$^{8.54}$ (superscripts denote the Ballesteros−Weinstein nomenclature),[47] located near the interface between transmembrane helix VII and amphipathic helix VIII. These residues are conserved among many class A GPCRs and form hydrophobic interactions with nearby residues in TM I, forming a local microswitch important to G protein signaling.[48] The chemical shift of the ^{19}F-NMR probe located at position 289 is sensitive to conformational changes in this microswitch region, which are linked to global structural changes between inactive and active conformational

https://doi.org/10.1021/jacs.4c15106
J. Am. Chem. Soc. 2025, 147, 17612−17625

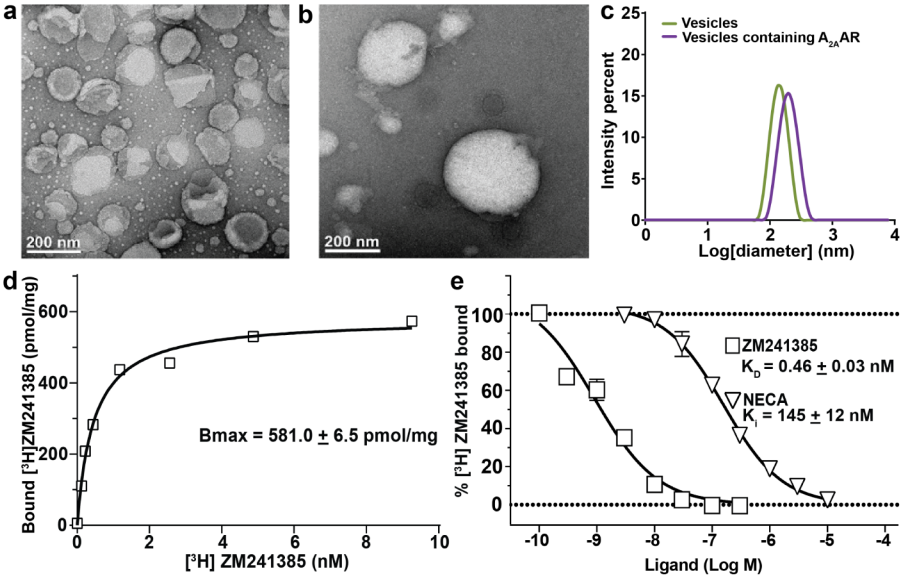

Figure 2. Characterization of lipid vesicles containing human $A_{2A}AR$ and pharmacological validation of $A_{2A}AR$ in vesicles. Representative negative stain electron micrographs of unilamellar vesicles composed of POPC and POPS (70:30 molar ratio) (a) without and (b) with reconstituted $A_{2A}AR$. (c) Dynamic light scattering measurements of the distribution of the sizes of vesicles composed of POPC and POPS (70:30 molar ratio) without (green) and with (purple) $A_{2A}AR$. (d and e) Pharmacological characterization of $A_{2A}AR$ in lipid vesicles. (d) Saturation binding experiment with ^3H[1]ZM241385 and $A_{2A}AR$ in lipid vesicles containing POPC and POPS (70:30 molar ratio). The reported B_{max} value represents the mean, and associated error is the s.e.m. from 3 independent trials done in triplicate. (e) Radioligand competition experiments. K_D and K_i values are reported for the antagonist ZM241385 and the agonist NECA, respectively. The reported error represents the s.e.m. from 3 independent trials done in triplicate.

states, as previously discussed[14,49] and described further below. Additionally, prior ^{19}F-NMR studies comparing $A_{2A}AR$-[A289C] in lipid nanodiscs and detergent micelles revealed highly similar chemical shifts across all conformational states in both membrane-mimetic environments.[15] This indicated that the ^{19}F-NMR probe detects shifts in the $A_{2A}AR$ conformational equilibria influenced by the membrane environment rather than responding directly to membrane composition changes.[15]

We developed a workflow to prepare phospholipid vesicles containing $A_{2A}AR$[A289C] for ^{19}F MAS NMR experiments (Figure 1). The workflow was based on earlier studies that reconstituted folded, detergent-solubilized transmembrane proteins into lipid vesicles.[50−52] The general approach was to first prepare vesicles of defined phospholipid composition and size and then destabilize the vesicles using detergent to facilitate insertion of purified, detergent-solubilized $A_{2A}AR$-[A289C], selectively remove the detergent, and homogenize the vesicles one final time before biochemical or NMR experiments (Figure 1). Phospholipid vesicles with and without reconstituted $A_{2A}AR$[A289C] were characterized as described in the following text.

To verify the formation of phospholipid vesicles, we recorded negative stain electron micrograph images of vesicles without and with reconstituted $A_{2A}AR$[A289C] (Figure 2a,b). Vesicle size was confirmed to be consistent with our expectations of ∼200 nm based on the pore size of 200 nm used for extrusion of the vesicles. Average vesicle diameters and distribution of vesicle sizes were confirmed in dynamic light scattering (DLS) experiments. Vesicles with and without reconstituted $A_{2A}AR$ were homogenous in size, with a polydispersity index of <0.1 for vesicles without $A_{2A}AR$ and a polydispersity index of <0.2 for vesicles containing $A_{2A}AR$ (Figure 2c).

To confirm the pharmacological function of $A_{2A}AR$[A289C] in lipid vesicles, we recorded radioligand saturation binding experiments and radioligand competition binding experiments (Figure 2d,e). In saturation binding experiments, increasing concentrations of [^3H]ZM241385 were incubated with POPC/POPS (70:30 molar ratio) vesicles containing $A_{2A}AR$-[A289C], and specific binding was determined as the difference in observed binding between samples prepared in the absence and presence of 10 μM cold ZM241385. From this method, we determined a B_{max} value for $A_{2A}AR$[A289C] in lipid vesicles to be 581.0 ± 6.5 pmol/mg (Figure 2d). This value is approximately a 22-fold increase in the amount of functional receptors as compared with $A_{2A}AR$ expressed in the plasma membranes of insect cells.[53] Importantly, these data confirmed that >95% of the receptors in our samples were pharmacologically active. For competition binding experiments, vesicle preparations were incubated with [^3H]-ZM241385 and increasing concentrations of cold ZM241385 or NECA. From competition binding experiments, we determined the affinities of $A_{2A}AR$[A289C] in POPC/POPS vesicles for a representative antagonist and agonist, determining a K_D of 0.46 nM for the antagonist ZM241385 and K_I for the agonist NECA of 145 nM (Figure 2e), nearly identical to the affinities determined for $A_{2A}AR$ in insect cells.[53]

The Orientation of $A_{2A}AR$ Inserted into Lipid Vesicles Depends on Lipid Composition and the Efficacy of Bound Ligands. Earlier structural characterization of membrane proteins in lipid vesicles has shown that integral membrane proteins can adopt multiple global orientations within vesicles.[54] Reconstituted $A_{2A}AR$ could potentially adopt two different global orientations: an "outward-facing" orientation, where the orthosteric binding pocket faces away from the vesicle interior, or an "inward-facing" orientation, where the orthosteric binding pocket is directed toward the

https://doi.org/10.1021/jacs.4c15106
J. Am. Chem. Soc. 2025, 147, 17612−17625

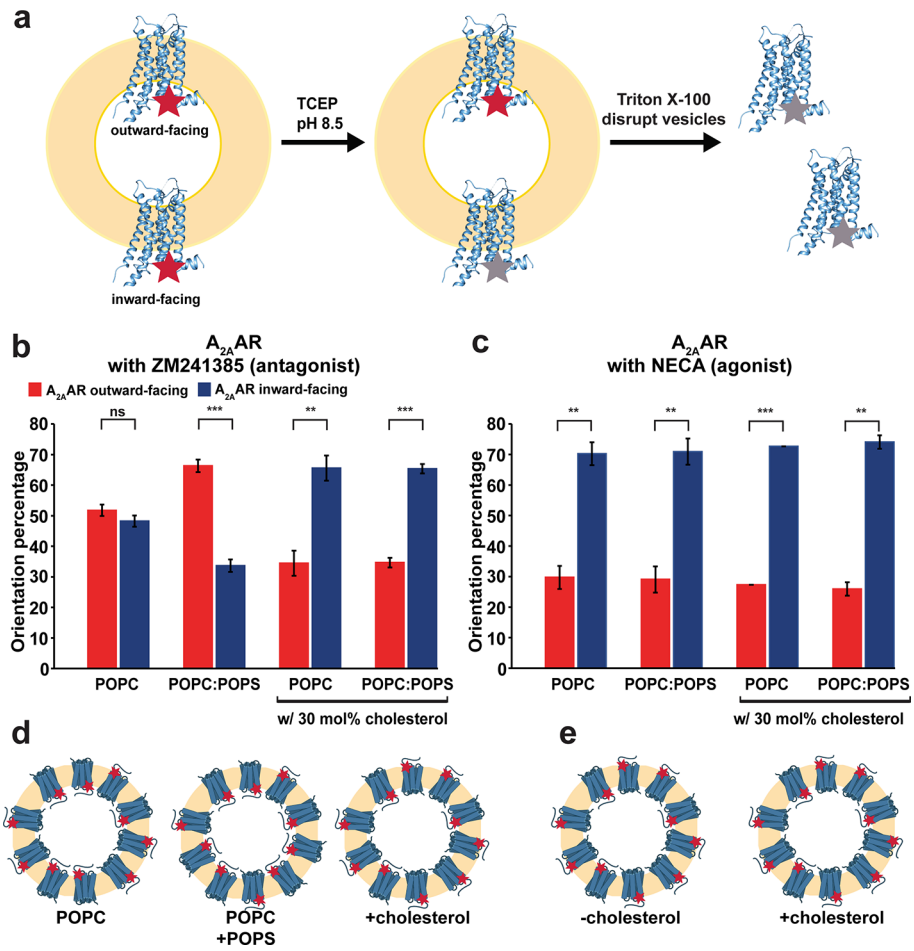

Figure 3. Determination of the orientation of $A_{2A}AR$ in vesicles of varying lipid compositions. (a) Schematic of the fluorescence-quenching assay used to quantify receptor orientation within vesicles. The red star represents position C289 labeled with Cy3. Receptors with Cy3 covalently attached to position C289 facing toward the vesicle interior are labeled "$A_{2A}AR$ inside", while receptors with Cy3 facing away from the vesicle interior are labeled "$A_{2A}AR$ outside". Gray stars represent Cy3-labels that have been chemically quenched. (b) Quantitative comparison of the orientation of the $A_{2A}AR$ complex with the antagonist ZM241385 in vesicles made from POPC or defined mixtures of POPC and POPS (70:30 molar ratio), POPC and 30 mol % cholesterol or POPC:POPS with 30 mol % cholesterol. The orientations "$A_{2A}AR$ inside" and "$A_{2A}AR$ outside" are defined in (a). (c) Quantitative comparison of the orientation of the $A_{2A}AR$ complex with the full agonist NECA in vesicles made from the same compositions as shown in (b) as labeled. The same color scheme as used in (b). Error bars indicate the s.e.m. calculated from $n \geq 3$ independent experiments. Statistically significant values are illustrated as $***p < 0.005$ using a 2-tailed unpaired *t*-test. (d and e) Schematics illustrating the orientation of $A_{2A}AR$ in lipid vesicles determined from the data shown in (b) and (c) for the $A_{2A}AR$ complexes with (d) antagonist ZM241385 and (e) full agonist NECA.

vesicle interior (Figure 3). To determine the orientation of $A_{2A}AR$[A289C] reconstituted in lipid vesicles, we adapted a previously reported protocol for quantifying the orientation of integral membrane proteins within phospholipid vesicles.[55] Following this method, a cyanine fluorophore was covalently attached to single solvent-accessible cysteine C289, the same position used for ^{19}F-TET labeling in NMR experiments, on $A_{2A}AR$ purified in detergent micelles. The labeled receptor was then reconstituted into vesicles, and the fluorescence intensity was measured. Next, a membrane-impermeable fluorescence quencher was introduced, and the resulting decrease of fluorescence reported on receptors oriented with the fluorescent dye facing outward, away from the vesicle. Finally, detergent was added to disrupt the vesicles, and fluorescence was measured again to quantify the receptors with an inward-facing orientation (Figure 3a). This approach was applied to quantify the orientation of $A_{2A}AR$[A289C] complexes with the antagonist ZM241385 and the full agonist NECA in vesicles composed of four different lipid compositions: POPC, a defined binary mixture of POPC and POPS at a 70:30 molar ratio, POPC with 30 mol % cholesterol, and a ternary mixture of POPC, POPS, and 30 mol % cholesterol.

For the $A_{2A}AR$[A289C] complex with the antagonist ZM241385 reconstituted into vesicles containing POPC, the orientation distribution was found to show a nearly equal distribution of outward-facing and inward-facing receptors (Figure 3b). In contrast to this, for the $A_{2A}AR$[A289C] complex with ZM241385 reconstituted into vesicles composed of POPC and POPS (70:30 molar ratio), approximately 70% of the receptors adopted an outward-facing orientation, while approximately 30% of the receptors adopted an inward-facing orientation (Figure 3b). For samples prepared with the $A_{2A}AR$[A289C] complex with ZM241385 in vesicles containing POPC and 30 mol % cholesterol or POPC, POPS, and 30 mol % cholesterol, the receptor adopted a different orientation preference, with approximately 70% of the receptors in an inward-facing orientation and 30% in an outward-facing orientation (Figure 3b).

https://doi.org/10.1021/jacs.4c15106
J. Am. Chem. Soc. 2025, 147, 17612−17625

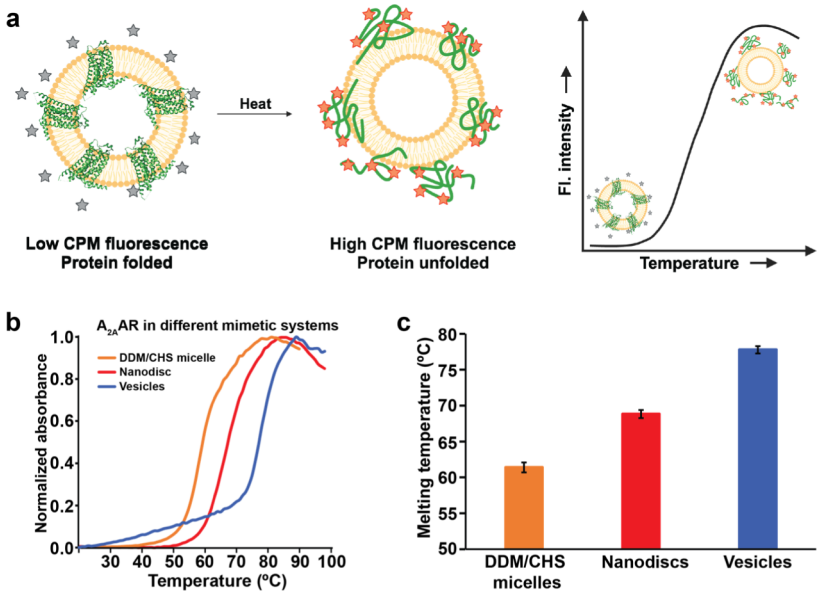

Figure 4. Fluorescence thermal melting profiles of the $A_{2A}AR$ complex with antagonist ZM241385 in three different membrane mimetics. (a) Schematic of the fluorescence thermal shift assay as applied to $A_{2A}AR$ in lipid vesicles. The inactive fluorescent dye (gray stars) shows increased emission upon covalent attachment with cysteines that become solvent accessible upon protein unfolding (orange stars). (b) Representative thermal melting profiles for $A_{2A}AR$ in DDM/CHS detergent micelles, lipid nanodiscs containing POPC and POPS (70:30 molar ratio), and lipid vesicles containing POPC and POPS (70:30 molar ratio). (c) The melting temperature for $A_{2A}AR$ in each membrane mimetic is reported as the mean of three independent experiments ± s.e.m.

Because the vesicles containing antagonist-bound receptors were prepared using identical protocols that created homogeneous vesicles of closely similar overall size, the differences observed in receptor orientation are unlikely to be due to variation in vesicle size. Instead, the receptor preference for an inward-facing orientation in vesicles composed of a binary mixture of POPC and POPS is more attributed to differences in membrane properties, such as lipid order[56,57] or local curvature induced by addition of POPS[58] or cholesterol (see Discussion section). Additionally, the asymmetry of receptor orientation in POPC/POPS vesicles suggests that the radioligand saturation data with the antagonist ZM241385 shown in Figure 2 may have undercounted the number of functional receptors. This is likely because ^{3}H-labeled antagonist ZM241385, like most other $A_{2A}AR$ ligands, may not fully penetrate the vesicles. Therefore, the estimated number of functional receptors in our NMR samples ranges from approximately 580 to 750 pmol/mg.

For the $A_{2A}AR$[A289C] complex with the full agonist NECA, we observed a significant difference in the orientation behavior compared to the complex with the antagonist ZM241385. For all lipid compositions, $A_{2A}AR$[A289C] in complex with NECA showed a clear orientation preference, with approximately 70% of the receptors adopting an inward-facing orientation and 30% of the receptors adopting an outward-facing orientation (Figure 3c). Only marginal variations were observed in the orientation preferences between different lipid compositions. The distinct orientation behavior between antagonist-bound and agonist-bound $A_{2A}AR$, particularly in vesicles without cholesterol, suggests that the receptor's orientation preference in lipid vesicles is influenced by the pharmacology of the bound ligand. This further indicates that the observed orientation preference is linked to the receptor's conformational equilibria, as further considered in the Discussion section.

Human $A_{2A}AR$ is More Thermally Stable in Lipid Vesicles Than in Nanodiscs or Detergent Micelles. To confirm that $A_{2A}AR$[A289C] reconstituted into lipid nanodiscs was globally folded, we recorded microscale fluorescence thermal melting assays by adapting a previously reported protocol for detergent-solubilized GPCRs.[59] This assay employs a thiol-reactive dye, 7-diethylamino-3-(4'-maleimidylphenyl)-4-methylcoumarin (CPM), which selectively interacts with cysteine residues from folded, buried regions of the protein that become solvent-accessible upon thermal unfolding. The fluorescence-based thermal melting assay has been used to assess receptor thermal stability in complexes with different ligands,[59,60] compare receptor stability in the presence of different ions,[61] compare receptor stability across various detergent micelle environments,[62] and evaluate the thermal stability of GPCRs reconstituted into lipid nanodiscs with distinct lipid compositions.[15]

$A_{2A}AR$[A289C] in complex with the antagonist ZM241385 reconstituted in vesicles composed of POPC and POPS (70:30 molar ratio) exhibited a thermal melting curve that showed a sharp transition from folded to unfolded proteins, indicating cooperative unfolding consistent with a folded receptor sample population (Figure 4). From these experiments, the melting temperature (T_M) of $A_{2A}AR$[A289C] in complex with the antagonist ZM241385 in lipid vesicles composed of POPC and POPS (70:30 molar ratio) was determined to be 77.8 ± 0.5 °C. This was found to be significantly higher than the melting temperatures of $A_{2A}AR$[A289C] in complex with ZM241385 in either lipid nanodiscs composed of the same ratio of POPC and POPS (T_M = 68.6 ± 0.5 °C) or in DDM/CHS mixed micelles (T_M = 61.2 ± 0.7 °C). Thus, the lipid vesicle environment provided the highest possible thermal stability for $A_{2A}AR$ among all membrane or membrane mimetic systems.

The Conformational Equilibrium of Antagonist-Bound $A_{2A}AR$ in Lipid Vesicles. We observed the

https://doi.org/10.1021/jacs.4c15106
J. Am. Chem. Soc. 2025, 147, 17612−17625

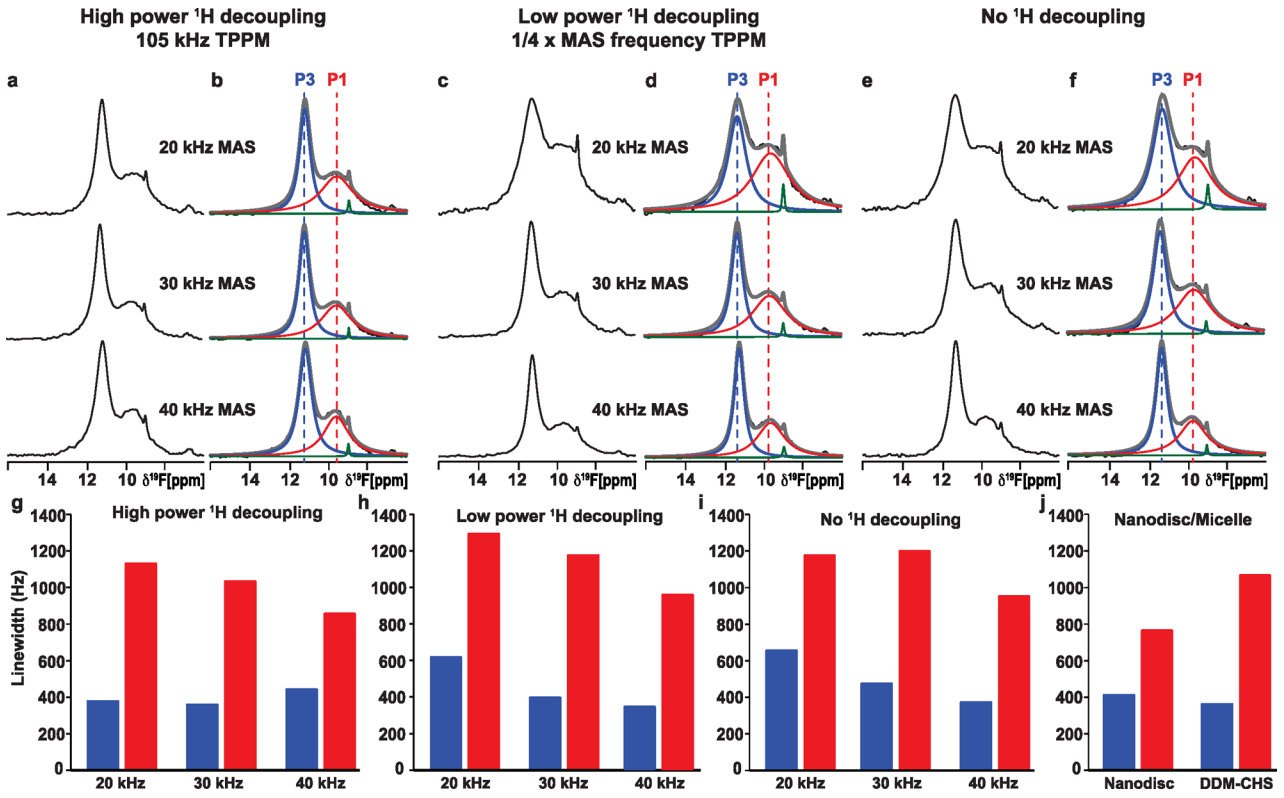

Figure 5. ^{19}F MAS NMR-observed conformational equilibria of human A_{2A}AR in complex with the antagonist ZM241385 in lipid vesicles measured with different experimental parameters. (a) One-dimensional ^{19}F-MAS spectra of A_{2A}AR[A289C^{TET}] in complex with the antagonist ZM241385 reconstituted into POPC/POPS lipid vesicles recorded with 105 kHz ^{1}H TPPM decoupling at three different MAS frequencies. (b) NMR spectra from (a) are shown superimposed with Lorentzian deconvolutions with the minimal number of components that provided a good fit, labeled P1 and P3. (c) One-dimensional ^{19}F-MAS spectra of the same sample recorded with ^{1}H TPPM decoupling power set to one-quarter of the applied MAS frequency. (d) NMR spectra from (c) are shown superimposed with Lorentzian deconvolutions with the minimal number of components that provided a good fit, labeled P1 and P3. (e) One-dimensional ^{19}F-MAS spectra of the same sample used recorded with no ^{1}H decoupling and (f) NMR spectra from (e) are shown superimposed with Lorentzian deconvolutions. Line widths measured for populations P1 and P3 for A_{2A}AR in (g–i) lipid vesicles or (j) lipid nanodiscs or detergent micelles. Components colored green are from free TET, consistent with earlier NMR studies (see the text).

conformational equilibria of A_{2A}AR[A289C^{TET}] in complex with the antagonist ZM241385 in lipid vesicles composed of a defined binary mixture of POPC and POPS (70:30 molar ratio) by utilizing the protocol from Figure 1. This lipid composition was selected to facilitate comparisons between the present solid-state NMR studies of A_{2A}AR[A289C^{TET}] in lipid vesicles and earlier solution NMR studies of A_{2A}AR-[A289C^{TET}] in detergent micelles[49] and lipid nanodiscs containing the same ratio of POPC and POPS.[14−16]

The ^{19}F-MAS NMR spectra of A_{2A}AR[A289C^{TET}] recorded at 20 kHz MAS with 105 kHz ^{1}H TPPM decoupling contained two signals at $\delta \approx 11.3$ ppm (P3) and $\delta \approx 9.5$ ppm (P1), with signal P3 being the largest signal in the spectrum (Figure 5a,b and S1). The nomenclature used to identify the individual components, "P1" and "P3," was used to be consistent with earlier ^{19}F-NMR observations of the conformational equilibria of A_{2A}AR.[49] In earlier studies, the spectral component "P3" was assigned to an inactive, antagonist-bound A_{2A}AR conformation based on the observations that this component was repeatedly observed in all spectra of A_{2A}AR bound to different antagonists but not observed in spectra of A_{2A}AR bound to agonists.[49] The spectral component "P1" had been observed in spectra of apo A_{2A}AR and in spectra of both antagonist-bound and agonist-bound A_{2A}AR and thus appeared to be present for both active and inactive conformational ensembles.[49] The chemical shifts of components P1 and P3 for spectra of antagonist-bound A_{2A}AR in lipid vesicles were observed to be nearly identical to the same spectral components for antagonist-bound A_{2A}AR in lipid nanodiscs[15] and in detergent micelles.[49] This indicated that the NMR probe at position 289C was not responsive to changes in the local membrane environment. Instead, the NMR probe at this position was responsive to changes in the A_{2A}AR conformational equilibria, which could be influenced by changes in the membrane environment.

The shape of the overall ^{19}F signal envelope, the number of observed spectral components, the chemical shifts of the two observed components, and the relative intensities of the populations P1 and P3 appeared highly similar between the solid-state preparation of antagonist-bound A_{2A}AR[A289C^{TET}] in lipid vesicles and antagonist-bound A_{2A}AR[A289C^{TET}] in lipid nanodiscs or detergent micelles in aqueous solutions (see below). With 105 kHz ^{1}H TPPM decoupling, we observed marginal decreases in the line widths for both components with increasing MAS frequency (Figure 5a,b,g), with a marginal increase in the line width for component P1 at 40 kHz MAS.

Previously reported SSNMR studies of microcrystalline amino acids and proteins demonstrated that at moderate to higher MAS frequencies, the application of low-power TPPM ^{1}H decoupling with an applied field of one-quarter of the MAS

https://doi.org/10.1021/jacs.4c15106
J. Am. Chem. Soc. 2025, 147, 17612−17625

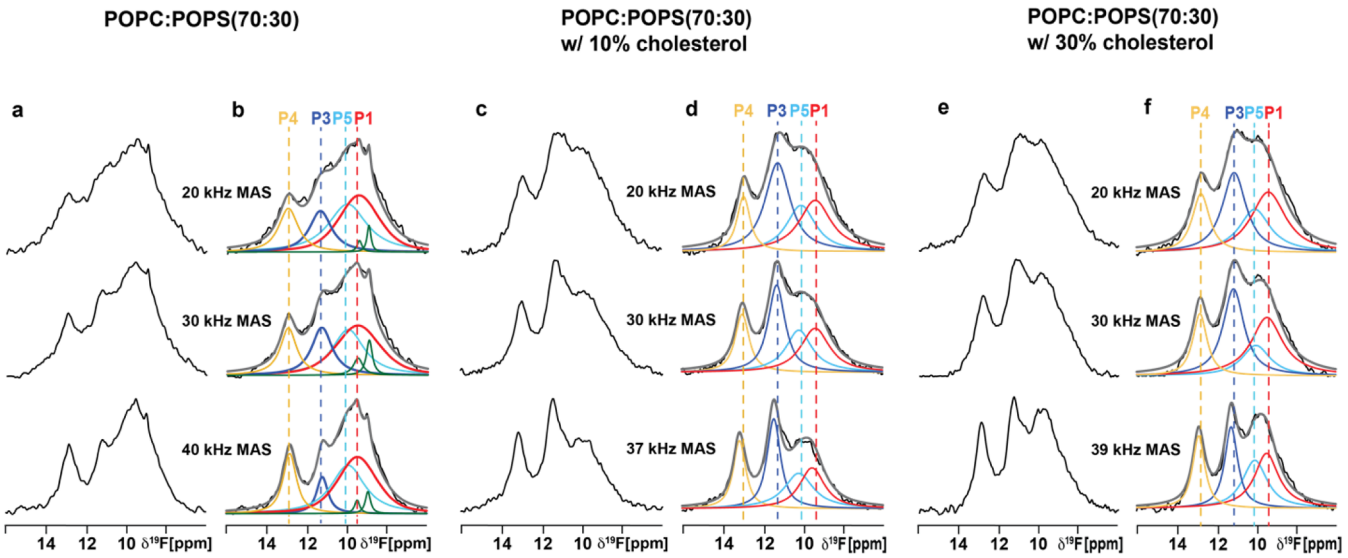

Figure 6. ^{19}F MAS NMR-observed conformational equilibria of human A_{2A}AR in complex with the agonist NECA in lipid vesicles of three different compositions measured at several MAS frequencies. (a) One-dimensional ^{19}F-MAS spectra of A_{2A}AR[A289C^{TET}] in complex with the agonist NECA in lipid vesicles composed of POPC and POPS (70:30 molar ratio) recorded for three different MAS frequencies and ^{1}H TPPM decoupling at an applied ^{1}H frequency of one-quarter of the MAS frequency. (b) NMR spectra from (a) are shown superimposed with Lorentzian deconvolutions with the minimal number of components that provided a good fit, labeled P1 through P5. Components colored green are from free TET, consistent with earlier NMR studies (see the text). (c–f) One-dimensional ^{19}F-MAS spectra and corresponding Lorentzian deconvolutions of A_{2A}AR[A289C^{TET}] in complex with the agonist NECA recorded for three different MAS frequencies and no ^{1}H decoupling in lipid vesicle samples composed of POPC, POPS (70:30 molar ratio) and (c and d) 10 mol % cholesterol or (e and f) 30 mol % cholesterol.

frequency was effective in providing high-resolution spectra in ^{13}C-detected experiments.[63,64] We tested whether ^{1}H TPPM decoupling with an applied field of one-fourth of the MAS frequency would produce spectra with resolution similar to that obtained with high-power TPPM decoupling. At 20 kHz MAS frequency, the lines in ^{19}F-NMR spectra recorded with low-power ^{1}H TPPM were about 20% broader than those observed at the same spinning frequency with high-power ^{1}H TPPM (Figure 5c,d,h). With increasing spinning frequency, we observed narrowing of both spectral components with low-power ^{1}H TPPM decoupling, from ∼1300 Hz for P1 and ∼620 Hz for P3 at 20 kHz MAS to ∼940 Hz for P1 and ∼340 Hz for P3 at 40 kHz MAS frequency (Figure 5c,d,h and Table S2). As a point of comparison, we also recorded ^{19}F MAS SSNMR spectra without any applied ^{1}H decoupling over the same range of MAS frequencies (Figure 5e,f). At a 20 kHz MAS frequency, we observed broader lines without decoupling, especially for component P3, which had a measured line width of ∼650 Hz (Table S2). At a 40 kHz MAS frequency, we observed significant narrowing for both components, ∼370 Hz for component P3 and ∼950 Hz for component P1 (Table S2), which was only marginally broader than the line width for P1 observed with low-power ^{1}H decoupling and high-power ^{1}H decoupling (Table S2). Considering the line widths for both components P1 and P3, we observed the overall best spectral resolution at 40 kHz MAS with low-power ^{1}H TPPM decoupling (Figure 5c,d).

We then used the optimal experimental conditions, 40 kHz MAS frequency, and low-power ^{1}H TPPM decoupling to compare the conformational equilibria of antagonist-bound A_{2A}AR[A289C^{TET}] across a range of sample temperatures (Figure S2). ^{19}F MAS SSNMR spectra were recorded for antagonist-bound A_{2A}AR[A289C^{TET}] in lipid vesicles containing POPC and POPS (70:30 molar ratio) at temperature set points ranging from 245 to 275 K. These temperatures represent the settings of the cooling unit and not the actual sample temperature. To obtain a more accurate measurement of the sample temperature, we accounted for the frictional heating caused by magic angle spinning, following established protocols that use the chemical shift of ^{79}Br in KBr powder.[65] At 40 kHz MAS, frictional heating was found to increase the sample temperature by approximately 40 °C. Therefore, the actual sample temperatures investigated were closer to 285 and 315 K. Because low-power ^{1}H TPPM deposits significantly less radiofrequency energy into the sample, the estimated sample temperatures accounting for frictional heating are likely very close to the actual sample temperatures. Across this temperature range, we observed only minor differences in the line widths or relative populations of the two components in all spectra of antagonist-bound A_{2A}AR[A289C^{TET}] (Figure S2).

The Conformational Equilibrium of Agonist-Bound A_{2A}AR in Lipid Vesicles. To investigate the conformational equilibria of agonist-bound A_{2A}AR[A289C^{TET}] in lipid vesicles, we prepared a sample in vesicles with the defined binary composition of POPC and POPS (70:30 molar ratio) in complex with the full agonist NECA, a high-affinity adenosine derivative (Figure 6). At 20 kHz MAS frequency, the ^{19}F-MAS NMR spectra of A_{2A}AR[A289C^{TET}] in complex with the agonist NECA contained multiple components with broader and partially overlapped lines (Figure 6). We observed the loss of population for component P2 and observed populations for components P1, P3, P4, and P5 in lipid nanodiscs.[15,49] We observed populations for components P1, P3, P4, and P5. From prior studies, component P4 has been assigned to an active conformation resembling that of A_{2A}AR in an active ternary signaling complex,[15] while component P5, typically observed for partial agonist complexes in lipid nanodiscs, was also detected in the full agonist complex within lipid vesicles. A complete deconvolution of the spectra required the inclusion of all of these components to achieve a satisfactory fit with the

https://doi.org/10.1021/jacs.4c15106
J. Am. Chem. Soc. 2025, 147, 17612−17625

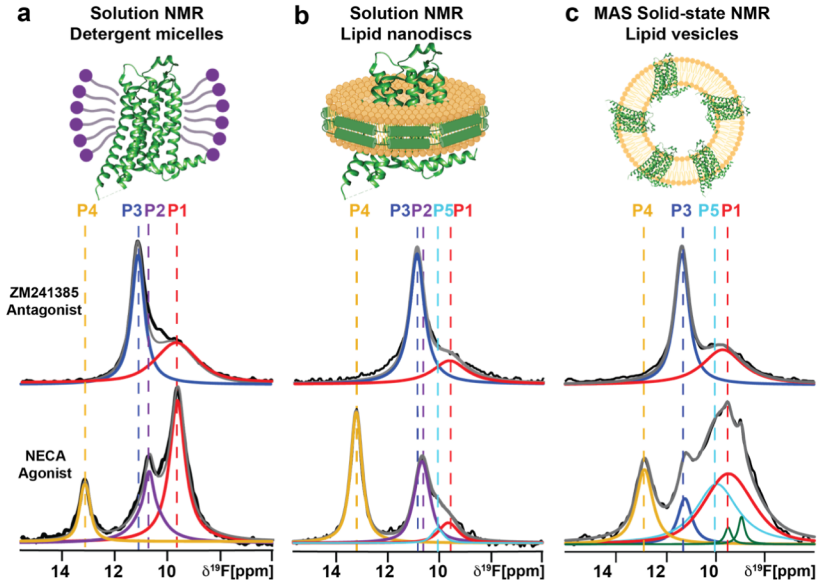

Figure 7. ^{19}F-NMR systematic comparison of the conformational equilibria of antagonist-bound and agonist-bound human $A_{2A}AR[A289C^{TET}]$ across three membrane or membrane-mimetic systems by solution NMR in (a) detergent micelles and (b) lipid nanodiscs and by MAS solid-state NMR in (c) lipid vesicles. The same color scheme as in Figures 5 and 6. All data were measured on the same spectrometer, with a magnetic field of 14.1 T, and near the same sample temperatures (see the text for details).

experimental data (Figure S3). Consistent with our observations of antagonist-bound $A_{2A}AR$, the chemical shifts of the individual components in the spectra of agonist-bound $A_{2A}AR$ were nearly identical between the solid-state preparation of agonist-bound $A_{2A}AR[A289C^{TET}]$ in lipid vesicles and agonist-bound $A_{2A}AR[A289C^{TET}]$ in lipid nanodiscs or detergent micelles in aqueous solutions (Figure 7). This further confirmed that the NMR probe at position A289 was sensitive to changes in the conformational equilibria of $A_{2A}AR$ but not directly sensitive to changes in the environment itself. Increasing the MAS frequency significantly improved the resolution, narrowing the line widths of all components at 30 kHz MAS and further at 40 kHz MAS (Figure 6). Between 20 and 40 kHz MAS, the line widths of most components were narrowed by 30% to 50%.

In earlier studies, the conformational equilibrium of agonist-bound $A_{2A}AR$ in lipid nanodiscs was shown to be temperature-dependent.[14] To investigate whether a similar effect occurred in lipid vesicles, we recorded ^{19}F-SSNMR spectra of agonist-bound $A_{2A}AR$ in lipid vesicles over temperatures ranging from 245 to 280 K (Figure S4). Accounting for frictional heating, the actual sample temperatures were closer to 285 to 315 K. At MAS frequencies of both 30 kHz and ∼40 kHz, increasing the temperature led to a proportional increase in the population of the active conformational state P4 and a corresponding decrease in the inactive conformational state P3 (Figure S4). This temperature-dependent shift in the conformational equilibrium of $A_{2A}AR$ in lipid vesicles qualitatively resembled that observed in lipid nanodiscs. However, the magnitude of the shift differed, as discussed further below.

We further investigated the conformational equilibria of agonist-bound $A_{2A}AR$ in two additional vesicle systems, the first composed of a defined ternary mixture of POPC, POPS, and 10 mol % cholesterol and the second composed of POPC, POPS, and 30 mol % cholesterol (Figure 6). Due to observed arcing in the MAS probe, ^{19}F-NMR spectra were recorded without ^{1}H decoupling, which resulted in only marginal increases in line widths over an MAS frequency range explored between 20 and 39 kHz. Comparable with the ^{19}F-NMR spectra of agonist-bound $A_{2A}AR$ in vesicles without cholesterol, spectra recorded in vesicles containing either 10 or 30 mol % cholesterol exhibited the same number of components with identical chemical shifts (Figure 6c–f). For the spectra in vesicles with 10 mol % cholesterol, we observed an increase in the active-state population P4, a reduction in the population P1, and an increase in the population P3 (Figure 6c,d). For the spectra in vesicles containing 30 mol % cholesterol, we observed a further increase in the population P4 and similar populations for other conformers (Figure 6e,f).

We also explored the temperature dependence of the agonist-bound $A_{2A}AR$ conformational equilibria in ^{19}F-SSNMR variable temperature spectra recorded with samples prepared in lipid vesicles containing cholesterol (Figures S5 and S6). In vesicles containing POPC, POPS, and either 10 or 30 mol % cholesterol, increasing the sample temperature resulted in an increase in the population of the active conformational state P4 and a corresponding decrease in the inactive conformational state P3 (Figures S5 and S6). The magnitude of this temperature-dependent response was less than what was observed for agonist-bound $A_{2A}AR$ in vesicles prepared without cholesterol (Figure S4).

Comparing the Conformational Equilibrium of $A_{2A}AR$ Across Three Different Membrane or Membrane-Mimetic Systems. The sensitivity and resolution obtained in ^{19}F MAS SSNMR spectra of lipid vesicle preparations of $A_{2A}AR[A289C^{TET}]$ complexes with both the antagonist ZM241385 and the agonist NECA approached the resolution observed in the spectra of $A_{2A}AR[A289C^{TET}]$ detergent or nanodisc preparations in aqueous solutions (Figure 7). The close agreement of the chemical shifts for all spectral components across all three studied systems—detergent micelles, lipid nanodiscs, and lipid vesicles—facilitated a direct comparison of the conformational equilibria of $A_{2A}AR$ across the three different membrane or membrane-mimetic systems. We compared ^{19}F-NMR spectra of $A_{2A}AR$ complexes with ZM241385 and NECA in lipid vesicles containing POPC and

https://doi.org/10.1021/jacs.4c15106
J. Am. Chem. Soc. 2025, 147, 17612−17625

POPS (70:30 molar ratio) to spectra of the same complexes in lipid nanodiscs with the same lipid composition and in detergent micelles composed of DDM and CHS (Figure 7). To ensure consistency, spectra were recorded at comparable temperatures, with solution NMR at 280 K and solid-state NMR at ∼285 K, with the same magnetic field (14.1 T) and on the same spectrometer running the same acquisition software (see Methods section).

For antagonist-bound $A_{2A}AR[A289C^{TET}]$, we observed highly similar spectra for the lipid vesicle, lipid nanodisc, and detergent micelle preparations. In all spectra, we observed two components, P1 and P3, that exhibited nearly identical chemical shifts. The relative intensities of both components and thus the relative population of each conformation varied only marginally across all sample conditions (Figure 7). This indicated that the conformational equilibria of antagonist-bound $A_{2A}AR$ were largely consistent between samples prepared in lipid vesicles and lipid nanodiscs of the same binary lipid composition and detergent micelles.

In contrast, for agonist-bound $A_{2A}AR[A289C^{TET}]$, we observed differences in the number of components in each spectrum among the different sample preparation conditions. The chemical shifts of the components remained nearly identical across all samples. Additionally, the relative populations of each component varied between lipid vesicles and the two membrane mimetic systems (Figure 7). This indicated that the conformational equilibrium of agonist-bound $A_{2A}AR$ was much more sensitive to changes in the membrane environment than that of antagonist-bound $A_{2A}AR$.

DISCUSSION

The radioligand saturation binding data shown in Figure 2 and the fluorescence thermal shift data shown in Figure 4 demonstrate advantages of structural and biophysical investigations of human receptor proteins in lipid vesicles, specifically the ability to generate homogeneous samples of pharmacologically active $A_{2A}AR$ that are more thermally stable than preparations in detergent micelles or lipid nanodiscs. GPCRs, and membrane proteins generally, are often difficult to work with because of their relatively lower thermal stability, prompting the development of alternative detergents and other membrane mimetics to facilitate biophysical studies.[66] The thermal stability data in Figure 4 show that vesicles provide an improved level of thermal stability for $A_{2A}AR$, and we anticipate that the benefits of vesicle preparations in providing a stabilizing environment can likely be extended to additional GPCRs. It is possible that the unilamellar vesicles become multilamellar upon exposure to the forces used for packing the MAS rotors and during magic angle spinning, though this did not appear to impact the receptor's response to bound ligands. We note that while the sample preparation scheme shown in Figure 1 provided reproducible samples, further optimization could be attempted in the future, such as the potential removal of the second extrusion step. Alternatives to the preparation scheme in Figure 1 may also be useful to test in future studies, for example, by adapting protocols used for preparing SSNMR samples of ion channels[67−69] by mixing detergent-solubilized lipids with folded proteins followed by dialysis to remove detergent and facilitate protein reconstitution into membranes.

Applying the protocol from Figure 1 to prepare samples of human $A_{2A}AR$ in lipid vesicles, we were able to record ^{19}F-NMR solid-state MAS spectra with resolution and sensitivity closely comparable to that obtained in solution with $A_{2A}AR$ in detergent micelles or lipid nanodiscs (Figures 5−7). This means we can record spectra with quality comparable to what we can obtain in solution with a similar amount of protein and similar experimental times, with the significant advantage that we can more closely replicate properties of the cellular membrane in lipid vesicles. In experimental conditions for spectra of antagonist-bound $A_{2A}AR[A289C^{TET}]$, measured with low-power TPPM ^1H decoupling and 40 kHz MAS frequency, the line width for component P1 was only ∼15% wider than the line width for the same component measured in lipid nanodiscs, and the line width for component P3 was slightly narrower in MAS SSNMR spectra than measured in lipid nanodiscs (Figure 5). For experiments using at least 30 kHz MAS frequency, spectra recorded without any ^1H decoupling were nearly identical in resolution to spectra recorded with ^1H TPPM decoupling and only marginally broader. The narrowing of line widths for both components with increasing MAS without ^1H decoupling suggested that the ^{19}F chemical shift anisotropy (CSA) was likely a larger contributing factor than $^1H-^{19}F$ dipolar couplings. We anticipate that by applying even higher MAS frequencies, we may expect to see additional line narrowing, as has been demonstrated in ^{19}F SSNMR experiments of model compounds recorded with MAS frequencies between 60 and 111 kHz.[70]

The fluorescence-based receptor orientation data in Figure 3 show that the $A_{2A}AR$ orientation is influenced by both the lipid composition of the vesicles and the efficacy of the bound ligand. When $A_{2A}AR$ is in complex with the antagonist ZM241385, no orientation preference was observed in vesicles composed solely of POPC. However, in vesicles containing binary mixtures of POPC and POPS, $A_{2A}AR$ exhibited a preference for the ligand-binding pocket to face away from the vesicle interior (Figure 3b). For vesicles composed of POPC, POPS, and 30 mol % cholesterol, this orientation preference was reversed, with the receptor orthosteric pocket favoring an inward-facing orientation toward the vesicle interior (Figure 3b). Previous studies have demonstrated that in synthetic vesicles with complex lipid compositions that include cholesterol, asymmetric lipid distributions naturally emerge, with cholesterol preferentially accumulating in the inner leaflet.[71,72] While the specific lipid ratios used in this study have not been explicitly examined for such asymmetry, these earlier findings suggest that cholesterol-driven leaflet asymmetry may be a general phenomenon in multicomponent vesicles. If present in our system, such an asymmetry across leaflets could contribute to the observed reorientation of antagonist-bound $A_{2A}AR$ in cholesterol-containing vesicles.

For $A_{2A}AR$ in complex with the full agonist NECA, we observe asymmetry in receptor orientations across all lipid compositions studied, where the receptor preferred to adopt an orientation with the orthosteric binding pocket facing toward the vesicle interior (Figure 3c). This preferred orientation was observed even for lipid compositions without cholesterol, where antagonist-bound $A_{2A}AR$ showed either no orientation preference or an opposite orientation preference (Figure 3b). A potential rationale for the orientation preference of agonist-bound $A_{2A}AR$ comes from the consideration of the conformational changes upon GPCR activation and the potential influence of bulk membrane properties on the activated receptor.

Upon agonist-stimulated activation, $A_{2A}AR$ undergoes a conformational change, with transmembrane helix VI exhibit-

https://doi.org/10.1021/jacs.4c15106
J. Am. Chem. Soc. 2025, 147, 17612−17625

ing a rotation and an ∼16 Å outward displacement at the intracellular surface (Figure 8). The displacement of helix VI

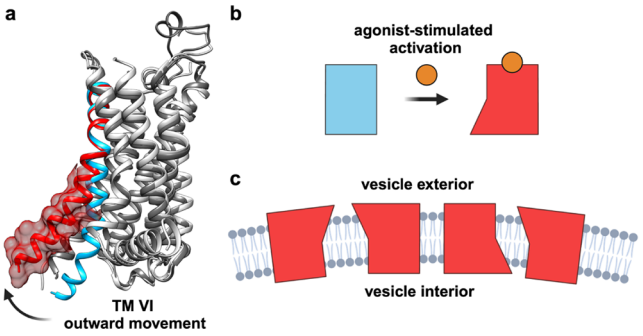

Figure 8. Agonist-stimulated $A_{2A}AR$ conformational changes influence the receptor orientation in lipid vesicles. (a) Superposition of crystal structures of inactive, antagonist-bound $A_{2A}AR$ (light gray, PDB 3EML) and active $A_{2A}AR$ from the ternary complex with an agonist and G protein (dark gray, PDB 5G53), as shown in ribbon representation. TM VI is colored blue for inactive $A_{2A}AR$ and red and shown superimposed on a space-filling representation for active $A_{2A}AR$. The arrow indicates the outward motion of TM VI upon agonist-stimulated activation. (b) Schematic illustrating that the agonist-stimulated activation of $A_{2A}AR$ results in the outward motion of TM VI increasing the size of the intracellular surface. (c) Schematic illustrating the orientation of agonist-bound $A_{2A}AR$ in lipid vesicles based on the orientation data shown in Figure 3.

results in an increased volume of ∼1300 to 1500 $Å^3$ at the intracellular surface of the active $A_{2A}AR$ conformation compared to the intracellular surface of inactive $A_{2A}AR$ (Figure 8). In contrast, the $A_{2A}AR$ extracellular surface does not undergo conformational rearrangements of the transmembrane helices between the inactive and active conformations. The difference in conformational responses between the intracellular and extracellular surfaces leads to a larger intracellular surface of the active conformation (Figure 8). It has been proposed that lateral pressures within lipid membranes contribute toward lipid-dependent changes in membrane protein function by influencing their conformational equilibria.[73,74] This effect is thought to depend on the three-dimensional shape of the integral membrane protein.[75,76] In our study, detergent-purified $A_{2A}AR$ was first equilibrated with the bound ligand prior to its reconstitution into lipid vesicles. Prior solution NMR studies of uniformly ^{2}H, ^{15}N-labeled $A_{2A}AR$ in detergent demonstrated that agonist-bound $A_{2A}AR$ adopted a structure highly similar to that of fully active $A_{2A}AR$ in a ternary signaling complex, which exhibits the outward movement of TM VI.[77] We hypothesize that the insertion of agonist-bound, active $A_{2A}AR$ proceeds in a way that minimizes the lateral pressures within the lipid membranes that act on the conformation of the active receptor, resulting in an asymmetric orientation within the vesicles (Figure 8).

When considered alongside the orientation data, the ^{19}F SSNMR data provide potential insights into the impact of membrane properties on the $A_{2A}AR$ conformational equilibria. This is evident when comparing ^{19}F SSNMR data of $A_{2A}AR$ with ^{19}F NMR data of $A_{2A}AR$ in soluble membrane mimetics, as shown in Figure 7. For antagonist-bound $A_{2A}AR$, the spectral envelope exhibited the same number of components with nearly identical chemical shifts in both solid-state lipid vesicle samples and aqueous solution preparations with DDM/CHS detergent micelles and lipid nanodiscs (Figure 7). This indicated that the conformational equilibria of antagonist-bound $A_{2A}AR$ near the intracellular surface are highly similar across all three environments. In contrast, for agonist-bound $A_{2A}AR$, we observed differences in the $A_{2A}AR$ conformational equilibria among the three different environments (Figure 7). At similar sample temperatures, $A_{2A}AR$ in lipid vesicles exhibited a spectrum more complex than that of $A_{2A}AR$ in lipid nanodiscs, with a relatively smaller active state population and increased populations for other conformational states (Figure 7). With increasing temperature, the conformational equilibria of agonist-bound $A_{2A}AR$ in POPC/POPS lipid vesicles became qualitatively more similar to that of agonist-bound $A_{2A}AR$ in lipid nanodiscs made from the same lipids, though with a relatively smaller active state conformation and larger P3 population (Figure S4). Since the comparisons between $A_{2A}AR$ in vesicles composed of POPC and POPS and nanodiscs composed of the same lipids were made with identical lipid compositions, it is unlikely that specific receptor-lipid interactions account for the differences in the conformational equilibria between the two membrane systems. Instead, these differences are more likely driven by variations in the bulk membrane properties, such as lateral pressure within the membrane. This opens intriguing avenues for further investigation, particularly in other GPCR systems, where variations in lipid properties, such as membrane curvature, could be systematically explored using vesicles to assess their impact on receptor conformational equilibria.

METHODS

Molecular Cloning. The gene encoding human $A_{2A}AR$ (1−316), cloned into a pPIC9K vector (Invitrogen) at the BamHI and NotI restriction sites, contained a single amino acid replacement (N154Q) to remove the only glycosylation site, an N-terminal FLAG tag, and a 10× C-terminal His tag. PCR-based site-directed mutagenesis was used to replace $A289^{7.54}$ with cysteine, creating $A_{2A}AR[A289C]$ using AccuPrime *Pfx* SuperMix (Thermo Fisher Scientific). The construct design is consistent with earlier studies,[15,16,49,78] and no new constructs were generated for this study.

$A_{2A}AR$ Production. Plasmids containing $A_{2A}AR[A289C]$ were transformed into the BG12 strain of *Pichia pastoris* (Biogrammatics) via electroporation. High-expressing clones were selected via a small-scale protein expression screening method where protein expression was evaluated by an anti-FLAG western blot assay, as previously reported.[78,79] Glycerol stocks of the highly expressing clones were prepared and stored at −80 °C for future use.

$A_{2A}AR$ was expressed in *P. pastoris* following previously published protocols.[15,78] 4 mL cultures in buffered minimal glycerol (BMGY) media were inoculated from glycerol stocks and grown at 30 °C for 48 h. These cultures were used to inoculate 50 mL of the BMGY medium and were grown at 30 °C for an additional 60 h. Next, the cultures were used to inoculate 500 mL of the BMGY medium and grown for 48 h at 30 °C. The cells were then harvested by centrifugation and resuspended in 500 mL of the buffered minimal methanol (BMMY) medium without methanol. The temperature was lowered to 28 °C, and no additional carbon source was added for 6 h to consume any remaining glycerol before protein expression was induced by the addition of methanol to a final concentration of 0.5% (w/v). Two more aliquots of methanol were added at 12 h intervals after induction, for a total expression time of 36 h. The cells were then harvested by

https://doi.org/10.1021/jacs.4c15106
J. Am. Chem. Soc. 2025, 147, 17612−17625

ultracentrifugation at 3000 × *g*, and the cell pellets were frozen in liquid nitrogen and stored at −80 °C for future use.

A_{2A}AR Purification and ^{19}F-Labeling via Chemical Modification. Purification and ^{19}F-labeling via an in-membrane chemical modification (IMCM) approach were carried out following previously reported protocols.[46] Cell pellets were resuspended in lysis buffer (100 mM NaCl, 50 mM sodium phosphate pH 7.0, 5% glycerol (w/v), and in-house prepared protease inhibitor solution) and lysed using a cell disruptor (Pressure Biosciences) at 40k PSI. Cell membranes containing A_{2A}AR[A289C] were isolated by ultracentrifugation at 200,000 × *g* for 30 min and homogenized in buffer (10 mM HEPES pH 7.0, 10 mM KCl, 20 mM $MgCl_2$, 1 M NaCl, and 4 mM theophylline). The homogenized membranes were incubated with 1 mM of 4,4'-dithiodipyridine (aldrithiol-4) and protease inhibitor cocktail solution (in-house prepared) for 1 h at 4 °C. Membrane suspensions were pelleted by ultracentrifugation at 200,000 × *g* for 30 min, and the supernatant was discarded to remove excess aldrithiol-4. The pelleted membranes were resuspended in the same buffer without aldrithiol-4 and incubated with 1 mM of 2,2,2-trifluoroethanethiol (TET) for 1 h at 4 °C. The suspended membranes were pelleted using ultracentrifugation at 200,000 × *g* for 30 min, resuspended in the same buffer without TET, and incubated with 1 mM theophylline and in-house prepared protease inhibitor solution for 30 min at 4 °C. The protein was extracted by mixing the resuspended membranes 1:1 (v/v) with solubilization buffer (50 mM HEPES pH 7.0, 500 mM NaCl, 0.5% (w/v) *n*-dodecyl-*β*-D-maltopyranoside (DDM), and 0.05% cholesteryl hemisuccinate (CHS)) for 6 h at 4 °C. The insolubilized material was separated by ultracentrifugation at 200,000 × *g* for 30 min, and the supernatant was incubated overnight at 4 °C with Co^{2+}-charged affinity resin (Talon, Clontech) and 30 mM imidazole.

After overnight incubation, the resin was washed with 20 CV of wash buffer 1 (50 mM HEPES pH 7.0, 10 mM $MgCl_2$, 30 mM imidazole, 500 mM NaCl, 8 mM ATP, 0.05% DDM, and 0.005% CHS) and twice with 20 CV each of wash buffer 2 (25 mM HEPES pH 7.0, 250 mM NaCl, 30 mM imidazole, 5% glycerol, 0.05% DDM, 0.005% CHS, and ligand). A_{2A}AR-[A289C] was eluted with buffer containing 50 mM HEPES pH 7.0, 250 mM NaCl, 300 mM imidazole, 5% glycerol, 0.05% DDM, 0.005% CHS, and ligand. The eluted protein was exchanged into buffer (25 mM HEPES pH 7.0, 75 mM NaCl, 0.05% DDM, 0.005% CHS, 100 *μ*M TFA, and ligand) by using a PD-10 desalting column (Cytiva) for use in all further experiments. All buffers were prepared with a saturating concentration of the ligand.

Preparation of Large Unilamellar Vesicles with and without A_{2A}AR. Phospholipids (POPC or mixtures of POPC and POPS) were dissolved in 2 mL of chloroform. The solution was then evaporated in a rotovap to make a lipid film and then vacuum-dried for 16 h. The lipids were resuspended via repeated vortexing in liposome buffer (25 mM HEPES pH 7.0, 75 mM NaCl, 100 *μ*M TFA, and ligand) to a final concentration of 1 mM. The lipid mixture was subjected to 9 freeze−thaw cycles to form multilamellar vesicles. Thawing was carried out in a water bath at a temperature of 10 °C above the highest transition temperature of the lipids used in the mixture. The multilamellar vesicles were then passed through an extruder with a 100 nM polycarbonate filter (Anatrace) 35 times to generate homogenous vesicles.

Vesicles containing A_{2A}AR were prepared by first mixing homogenous vesicles with dI H_2O containing 0.25% DDM and 0.025% CHS for 4 h with gentle rotation at room temperature. The purified receptor was then added to maintain a lipid-to-protein (L/P) molar ratio of 40:1 and allowed to incubate at 4 °C for 4 h. Following this, the sample was then mixed with prewashed bio-beads (Bio-Rad Laboratories) and incubated for 12−16 h at 4 °C. The bio-beads were removed, and the vesicles were passed through an extruder 11 times. These samples were then used for further experiments.

Dynamic Light Scattering (DLS) Measurements. Lipid vesicles without and with reconstituted A_{2A}AR were prepared as described above and diluted one-to-one by volume with liposome buffer (25 mM HEPES pH 7.0, 75 mM NaCl) to prevent multiple scattering events. DLS experiments were carried out using a Malvern Zetasizer Nano-ZS instrument maintained at 25 °C with cuvettes containing 1.0 mL of vesicles in buffer. The duration of each experiment was 60 seconds. The intensity distributions were calculated with Zetasizer Software 7.3 (Malvern Panalytical). The polydispersity index of the samples used in this study was maintained at less than 0.1. For each reported data set, three replicates were prepared, and each measurement was performed in triplicate (i.e., 9 measurements in total) to ensure reproducibility.

Receptor Orientation in Vesicles. The orientation of A_{2A}AR[A289C] in LUVs was quantified by adapting a previously described protocol.[55] A_{2A}AR[A289C] was purified in aqueous buffer containing DDM/CHS and in complex with ZM241385, as described above, and position C289 was labeled via maleimide chemistry with DY647P1-03 (Dynomics GmbH, Jena, Germany). The purified protein was incubated with a 10 molar excess of DY647P1-03 for 3 h at 4 °C in the dark. The reaction was stopped by diluting the sample with 5× volume of buffer without dye (25 mM HEPES pH 7.0, 75 mM NaCl, 0.05% DDM, 0.005% CHS, and ligand), and the excess dye was removed by buffer exchange through a PD10 column (Cytiva). The labeled A_{2A}AR[A289C] sample was reconstituted into vesicles using the above-described protocol. The sample fluorescence intensity was monitored using a BMG plate-reader with an excitation wavelength of 640 nm and an emission wavelength of 700 nm. 14 mM TCEP (pH 9.0) was added and incubated for 15 min, and the fluorescence intensity was measured again. After 5 min, a solution of 50% Triton X-100 was added to reach a final concentration of 0.05% Triton X-100 in the sample and allowed to equilibrate for 5 min to disrupt the vesicles. After 5 min, the fluorescence intensity was measured again. The orientation of the receptor was calculated from the ratio of the two consecutive quenching steps.

Electron Microscopy Imaging. Liposome samples were prepared with ZM241385 as described above, and the samples were diluted 5× in buffer containing 25 mM HEPES pH 7.0 and 75 mM NaCl. Glow-discharged 400 mesh carbon-coated Formvar copper grids (FCF400CU-UB, Electron Microscopy Sciences, Hatfield, PA) were floated onto 5 *μ*L of sample for 5 min. The grid was then transferred to a drop of deionized water for 5 s, and then, the excess solution was blotted from the grid with filter paper. The sample grid was then floated onto a drop of 1% aqueous uranyl acetate (Mallinckrodt, St. Louis, MO) for 30 s and then blotted dry. The grids were examined with a FEI Tecnai G2 Spirit Twin TEM (FEI Corp., Hillsboro, OR), and digital images were acquired with a Gatan UltraScan 2k × 2k camera and Digital Micrograph software

https://doi.org/10.1021/jacs.4c15106
J. Am. Chem. Soc. 2025, 147, 17612−17625

(Gatan Inc., Pleasanton, CA). The images were processed and analyzed using ImageJ.[80]

Radioligand Binding Experiments and Data Analysis. Saturation binding and competition binding experiments were recorded following previously described protocols.[15,81] For saturation binding experiments, increasing concentrations of [^{3}H]ZM241385 (250 μCi/mmol, Revvity) from 0.1 to 20 nM were incubated with 0.1 μg of liposomes containing A_{2A}AR-[A289C] at 25 °C in buffer containing 25 mM HEPES pH 7.0 and 75 mM NaCl. Specific binding of A_{2A}AR[A289C] was determined as the difference in observed binding between samples prepared in the absence and presence of 10 μM ZM241385. All experiments were conducted with three or more replicates. The K_D and B_{max} values were determined by fitting the data to a one site binding model in Prism 8 (GraphPad Software, Inc.).

For competition binding experiments, vesicle preparations were incubated with [^{3}H]-ZM241385 (2 nM, Revvity) and increasing concentrations of cold ZM241385 or NECA at 25 °C for 60 min in buffer containing 25 mM HEPES (pH 7.0) and 75 mM NaCl. Binding reactions were terminated by filtration through PerkinElmer Easytab-C self-aligned filtermats under reduced pressure using a FilterMat universal harvester (Revvity) and followed by washing twice with 1 mL cold buffer. Radioactivity was measured using a MicroBeta2 microplate scintillation counter (Revvity). All competition binding experiments were conducted with three or more replicates. IC_{50} values were determined using nonlinear, least-squares regression analysis (Prism 8; GraphPad Software, Inc.). The IC_{50} values were converted to K_I values using the Cheng–Prusoff equation.[82] Error bars for each measurement were calculated as the standard error of mean (s.e.m.) for experiments done in triplicate.

MAS SSNMR Sample Preparation. Vesicles containing A_{2A}AR[A289C] were pelleted by centrifugation at 200,000 × g for 1 h. The pellet was then packed into a Bruker 1.9 mm rotor by centrifugation at 20,000 × g for 60 min using a series of micropipette tips inserted into the rotor. The total mass for each sample, including lipids, receptor, and aqueous buffer, weighed approximately 15 mg.

^{19}F NMR Spectroscopy. All ^{19}F-SSNMR spectra were recorded by using a Bruker Avance III HD spectrometer operating at 600 MHz ^{1}H precession frequency using TopSpin 3.6.2 and equipped with a Bruker 1.9 mm ^{1}H/^{19}F/X/Y MAS probe. The flow rate was maintained at 800 liters per hour or higher to maintain temperatures. The 90° ^{19}F channel pulse length was 2.33 μs. Two-pulse phase-modulated (TPPM)[83] decoupling or alternative ^{1}H decoupling schemes were applied during the acquisition period, as described in the main text. The heteronuclear decoupling sequence TPPM15 (for 20 and 30 kHz MAS) was used at both high-power (105 kHz) and low-power (1/4 MAS) ^{1}H decoupling during acquisition. A 30° phase cycling (−15° to 15°) was used for the TPPM sequence for data collection at 40 kHz MAS. Spectra were recorded with a data size of 4k complex points, with an acquisition period of 147 μs, 11k scans, 3.6 μs dwell time, and 2 s recycle delay for a total experimental time of about 6 h per experiment.

An estimation of the sample temperature and calibration of the contribution of frictional heating to the sample temperature was obtained by measuring the ^{79}Br chemical shift and spin–lattice relaxation time in a sample of powdered KBr at multiple spinning frequencies following previous protocols.[65]

^{19}F-NMR solution experiments were recorded with the same magnet and console as the SSNMR experiments, equipped with a Bruker 5 mm BBFO probe. Temperatures were calibrated from a standard sample of 4% methanol in D4-MeOH. One-dimensional ^{19}F-NMR data were recorded with a data size of 32k complex points, with an acquisition period of 360 ms, a 120 ms dwell time, and 0.3 s recycle delay for a total experimental time of ∼3.5 h per experiment.

NMR Data Analysis. All NMR data were processed identically in TopSpin 4.0.8 (Bruker BioSpin). The ^{19}F-NMR data were zero-filled to 32k points and multiplied by an exponential window function with 60 Hz line broadening prior to Fourier transformation. ^{19}F-NMR spectra were referenced to the signal from trifluoroacetic acid (TFA) at −75.8 ppm, which was set to 0 ppm. Deconvolution of the ^{19}F-NMR data followed previously published procedures and was done with MestreNova version 14.1.1-24571 (Mestrelab Research). Following previously published procedures,[14−16] for each spectrum, the residual difference between the experimental data and the sum of the deconvoluted signals was assessed to check the quality of the deconvolution. The relative population of the different A_{2A}AR conformational states was calculated as a ratio of the integrated area of each deconvoluted peak to the total integral of all the signals from 6 to 16 ppm.

■ ASSOCIATED CONTENT

Data Availability Statement

Data used for analysis or generation of figures in this manuscript are available upon request.

Supporting Information

The Supporting Information is available free of charge at https://pubs.acs.org/doi/10.1021/jacs.4c15106.

Additional ^{19}F one-dimensional NMR spectra of antagonist-bound and agonist-bound A_{2A}AR measured at variable MAS frequencies, variable temperatures, and with different decoupling schemes; tables of measured line widths of deconvoluted components from ^{19}F-NMR spectra; and tables of relative populations of deconvoluted components from ^{19}F-NMR spectra (PDF)

■ AUTHOR INFORMATION

Corresponding Author

Matthew T. Eddy − *Department of Chemistry, University of Florida, Gainesville, Florida 32611, United States;* orcid.org/0000-0002-3349-6212; Email: matthew.eddy@ufl.edu

Authors

Arka Prabha Ray − *Department of Chemistry, University of Florida, Gainesville, Florida 32611, United States*

Beining Jin − *Department of Chemistry, University of Florida, Gainesville, Florida 32611, United States*

Complete contact information is available at: https://pubs.acs.org/10.1021/jacs.4c15106

Author Contributions

#A.P.R. and B.J. have contributed equally to this work. M.T.E. designed the study. B.J. and A.P.R. performed protein production, purification, and vesicle sample preparation. A.P.R. and B.J. recorded and analyzed NMR data with input from M.T.E. M.T.E., B.J., and A.P.R. wrote the manuscript.

Notes

The authors declare no competing financial interest.

■ ACKNOWLEDGMENTS

This work was supported by the National Institutes of Health, NIGMS MIRA grant R35GM138291 (M.T.E., B.J., and A.P.R.) and by an NIH equipment supplemental grant R35GM138291-03S2. A portion of this work was supported by an NIH award, S10 OD028753, for magnetic resonance instrumentation. The authors also acknowledge the UF ICBR Electron Microscopy Core, RRID:SCR_019146.

■ REFERENCES

(1) Xu, P.; et al. Structural insights into the lipid and ligand regulation of serotonin receptors. *Nature* **2021**, *592*, 469−473.
(2) Zhang, M.; et al. Cryo-EM structure of an activated GPCR−G protein complex in lipid nanodiscs. *Nat. Struct. Mol. Biol.* **2021**, *28*, 258−267.
(3) Yin, J.; et al. Structure of a D2 dopamine receptor−G-protein complex in a lipid membrane. *Nature* **2020**, *584*, 125−129.
(4) Staus, D. P.; et al. Structure of the M2 muscarinic receptor−β-arrestin complex in a lipid nanodisc. *Nature* **2020**, *579*, 297−302.
(5) Kim, Y.; et al. Bitter taste receptor activation by cholesterol and an intracellular tastant. *Nature* **2024**, *628*, 664−671.
(6) Patil, D. N.; et al. Cryo-EM structure of human GPR158 receptor coupled to the RGS7-Gβ5 signaling complex. *Science* **2022**, *375*, 86−91.
(7) Song, W.; Yen, H.-Y.; Robinson, C. V.; Sansom, M. S. P. State-dependent lipid interactions with the A2A receptor revealed by MD simulations using in vivo-mimetic membranes. *Structure* **2019**, *27*, 392−403.
(8) Yen, H.-Y.; et al. PtdIns(4,5)P2 stabilizes active states of GPCRs and enhances selectivity of G-protein coupling. *Nature* **2018**, *559*, 423−427.
(9) Damian, M.; et al. Allosteric modulation of ghrelin receptor signaling by lipids. *Nat. Commun.* **2021**, *12*, 1−15.
(10) Eberle, S. A.; Gustavsson, M. Bilayer lipids modulate ligand binding to atypical chemokine receptor 3. *Structure* **2024**, *32*, 1174−1183.E5.
(11) Yang, L.; Lyman, E. Local Enrichment of Unsaturated Chains around the A_{2A} Adenosine Receptor. *Biochemistry* **2019**, *58*, 4096−4105.
(12) Huang, S. K.; et al. Allosteric modulation of the adenosine A2A receptor by cholesterol. *eLife* **2022**, *11*, No. e73901.
(13) Mizumura, T.; et al. Activation of adenosine A_{2A} receptor by lipids from docosahexaenoic acid revealed by NMR. *Sci. Adv.* **2020**, *6*, No. eaay8544.
(14) Thakur, N.; et al. Membrane mimetic-dependence of GPCR energy landscapes. *Structure* **2024**, *32*, 523−535.e5.
(15) Thakur, N.; Ray, A. P.; Sharp, L.; Jin, B.; Duong, A.; Pour, N. G.; Obeng, S.; Wijesekara, A. V.; Gao, Z.-G.; et al. Anionic phospholipids control mechanisms of GPCR-G protein recognition. *Nat. Commun.* **2023**, *14*, 794.
(16) Ray, A. P.; Thakur, N.; Pour, N. G.; Eddy, M. T. Dual mechanisms of cholesterol-GPCR interactions that depend on membrane phospholipid composition. *Structure* **2023**, *31*, P836−847.E6.
(17) Van Aalst, E. J.; McDonald, C. J.; Wylie, B. J. Cholesterol biases the conformational landscape of the chemokine receptor CCR3: A MAS SSNMR-filtered molecular dynamics study. *J. Chem. Inf. Model.* **2023**, *63*, 3068−3085.
(18) García-Nafría, J.; Tate, C. G. Structure determination of GPCRs: cryo-EM compared with X-ray crystallography. *Biochem. Soc. Trans.* **2021**, *49*, 2345−2355.
(19) García-Nafría, J.; Tate, C. G. Cryo-EM structures of GPCRs coupled to Gs, Gi and Go. *Mol. Cell. Endocrinol.* **2019**, *488*, 1−13.
(20) Dawaliby, R.; et al. Allosteric regulation of G protein−coupled receptor activity by phospholipids. *Nat. Chem. Biol.* **2016**, *12*, 35−39.
(21) Shimada, I.; Ueda, T.; Kofuku, Y.; Eddy, M. T.; Wüthrich, K. GPCR drug discovery: Integrating solution NMR data with crystal and cryo-EM structures. *Nat. Rev. Drug Disc.* **2019**, *18*, 59−82.
(22) Jones, A. J. Y.; Gabriel, F.; Tandale, A.; Nietlispach, D. Structure and dynamics of GPCRs in lipid membranes: physical principles and experimental approaches. *Molecules* **2020**, *25*, 4729.
(23) Denisov, I. G.; Grinkova, Y. V.; Lazarides, A. A.; Sligar, S. G. Directed self-assembly of monodisperse phospholipid bilayer nanodiscs with controlled size. *J. Am. Chem. Soc.* **2004**, *126*, 3477−3487.
(24) Hagn, F.; Etzkorn, M.; Raschle, T.; Wagner, G. Optimized phospholipid bilayer nanodiscs facilitate high-resolution structure determination of membrane proteins. *J. Am. Chem. Soc.* **2013**, *135*, 1919−1925.
(25) Zhao, C. Limitations in membrane protein structure determination by lipid nanodiscs. *Trends Biochem. Sci.* **2024**, *49*, 475−476.
(26) Rosholm, K. R.; et al. Membrane curvature regulates ligand-specific membrane sorting of GPCRs in living cells. *Nat. Chem. Biol.* **2017**, *13*, 724−729.
(27) Real Hernandez, L. M.; Levental, I. Lipid packing is disrupted in copolymeric nanodiscs compared with intact membranes. *Biophys. J.* **2023**, *122*, 2256−2266.
(28) You, X.; Thakur, N.; Ray, A. P.; Eddy, M. T.; Baiz, C. R. A comparative study of interfacial environments in lipid nanodiscs and vesicles. *Biophys. Rep.* **2022**, *2*, 100066.
(29) Martinez, D.; et al. Lipid internal dynamics probed in nanodiscs. *ChemPhyschem* **2017**, *18*, 2651−2657.
(30) Stepien, P.; Polit, A.; Wisniewska-Becker, A. Comparative EPR studies on lipid bilayer properties in nanodiscs and liposomes. *Biochim. Biophys. Acta, Biomembr.* **2015**, *1848*, 60−66.
(31) Mörs, K.; et al. Modified lipid and protein dynamics in nanodiscs. *Biochim. Biophys. Acta, Biomembr.* **2013**, *1828*, 1222−1229.
(32) Dalal, V.; et al. Lipid nanodisc scaffold and size alter the structure of a pentameric ligand-gated ion channel. *Nat. Commun.* **2024**, *15*, 25.
(33) Strickland, K. M.; Neselu, K.; Grant, A. J.; Espy, C. L.; McCarty, N. A.; Schmidt-Krey, I. et al. Reconstitution of detergent-solubilized membrane proteins into proteoliposomes and nanodiscs for functional and structural studies.In *Structure And Function Of Membrane Proteins*; Springer, 2021, Vol; *2302*, pp. 21−35. DOI: .
(34) Huang, S. K.; et al. Delineating the conformational landscape of the adenosine A2A receptor during G protein coupling. *Cell* **2021**, *184*, 1884−1894.
(35) Ye, L.; Van Eps, N.; Zimmer, M.; Ernst, O. P.; Scott Prosser, R. Activation of the A2A adenosine G-protein-coupled receptor by conformational selection. *Nature* **2016**, *533*, 265−268.
(36) Clark, L.; Dikiy, I.; Rosenbaum, D. M.; Gardner, K. H. On the use of Pichia pastoris for isotopic labeling of human GPCRs for NMR studies. *J. Biomol. NMR* **2018**, *71*, 203−211.
(37) Clark, L. D.; et al. Ligand modulation of sidechain dynamics in a wild-type human GPCR. *eLife* **2017**, *6*, No. e28505.
(38) Shi, P.; et al. *In situ* ^{19} F NMR studies of an E. coli membrane protein. *Protein Sci.* **2012**, *21*, 596−600.
(39) Grage, S. L.; Wang, J.; Cross, T. A.; Ulrich, A. S. Solid-state 19F-NMR analysis of 19F-labeled tryptophan in gramicidin A in oriented membranes. *Biophys. J.* **2002**, *83*, 3336−3350.
(40) Su, Y.; DeGrado, W. F.; Hong, M. OrientationDynamics, and Lipid Interaction of an Antimicrobial Arylamide Investigated by ^{19} F and ^{31} P Solid-State NMR Spectroscopy. *J. Am. Chem. Soc.* **2010**, *132*, 9197−9205.
(41) Su, Y.; Doherty, T.; Waring, A. J.; Ruchala, P.; Hong, M. Roles of arginine and lysine residues in the translocation of a cell-penetrating peptide from ^{13}C, ^{31}P, and ^{19}F solid-state NMR. *Biochemistry* **2009**, *48*, 4587−4595.
(42) Kumar, K.; et al. 19F solid-state NMR approaches to probe antimicrobial peptide interactions with membranes in whole cells. *Biochim. Biophys. Acta, Biomembr.* **2024**, *1866*, 184269.
(43) Grage, S. L.; Kara, S.; Bordessa, A.; Doan, V.; Rizzolo, F.; Putzu, M.; Kubař, T.; Papini, A. M.; Chaume, G.; Brigaud, T.; et al.

Orthogonal ^{19}F-Labeling for Solid-State NMR Spectroscopy Reveals the Conformation and Orientation of Short Peptaibols in Membranes. *Chem. - Eur. J.* **2018**, *24*, 4328−4335.
(44) Duan, P.; et al. Binding sites of a positron emission tomography imaging agent in Alzheimer's β-amyloid fibrils studied using ^{19}F solid-state NMR. *J. Am. Chem. Soc.* **2022**, *144*, 1416−1430.
(45) Lu, M.; et al. ^{19}F dynamic nuclear polarization at fast magic angle spinning for NMR of HIV-1 capsid protein assemblies. *J. Am. Chem. Soc.* **2019**, *141*, 5681−5691.
(46) Sušac, L.; O'Connor, C.; Stevens, R. C.; Wüthrich, K. In-membrane chemical modification (IMCM) for site-specific chromophore labeling of GPCRs. *Angew. Chem., Int. Ed.* **2015**, *127*, 15461−15464.
(47) Ballesteros, J. A.; Weinstein, H. Integrated methods for the construction of three-dimensional models and computational probing of structure-function relations in G protein-coupled receptors. In *Methods in Neurosciences*; Elsevier, 1995, Vol. *25*, pp. 366−428. DOI: .
(48) Lu, S.; et al. Activation pathway of a G protein-coupled receptor uncovers conformational intermediates as targets for allosteric drug design. *Nat. Commun.* **2021**, *12*, 4721.
(49) Sušac, L.; Eddy, M. T.; Didenko, T.; Stevens, R. C.; Wüthrich, K. A2A adenosine receptor functional states characterized by 19F-NMR. *Proc. Natl. Acad. Sci. U. S. A.* **2018**, *115*, 12733−12738.
(50) Dijkman, P. M.; et al. Dynamic tuneable G protein-coupled receptor monomer-dimer populations. *Nat. Commun.* **2018**, *9*, 1710.
(51) Goddard, A. D.; Dijkman, P. M.; Adamson, R. J.; Dos Reis, R. I.; Watts, A. Reconstitution of Membrane Proteins: A GPCR as an Example *Methods in Enzymology*; Elsevier, 2015, Vol. *556*, pp. 405−424. DOI: .
(52) Rigaud, J.-L.; Lévy, D.*Methods in Enzymology*; Elsevier, 2003, *372*, pp.65−86.DOI: .
(53) Jaakola, V.-P.; et al. The 2.6 angstrom crystal structure of a human A_{2A} adenosine receptor bound to an antagonist. *Science* **2008**, *322*, 1211−1217.
(54) Tao, X.; Zhao, C.; MacKinnon, R. Membrane protein isolation and structure determination in cell-derived membrane vesicles. *Proc. Natl. Acad. Sci. U. S. A.* **2023**, *120*, No. e2302325120.
(55) Deutschmann, S.; Rimle, L.; Von Ballmoos, C. Rapid Estimation of Membrane Protein Orientation in Liposomes. *ChemBiochem* **2022**, *23*, No. e202100543.
(56) Leftin, A.; Molugu, T. R.; Job, C.; Beyer, K.; Brown, M. F. Area per lipid and cholesterol interactions in membranes from separated local-field 13C NMR spectroscopy. *Biophys. J.* **2014**, *107*, 2274−2286.
(57) Żak, A.; Korshunova, K.; Rajtar, N.; Kulig, W.; Kepczynski, M. Deciphering lipid arrangement in phosphatidylserine/phosphatidylcholine mixed membranes: simulations and experiments. *Langmuir* **2023**, *39*, 18995−19007.
(58) Koldsø, H.; Shorthouse, D.; Hélie, J.; Sansom, M. S. Lipid clustering correlates with membrane curvature as revealed by molecular simulations of complex lipid bilayers. *PloS Comput. Biol.* **2014**, *10*, No. e1003911.
(59) Alexandrov, A. I.; Mileni, M.; Chien, E. Y. T.; Hanson, M. A.; Stevens, R. C. Microscale fluorescent thermal stability assay for membrane proteins. *Structure* **2008**, *16*, 351−359.
(60) Xu, F.; Wu, H.; Katritch, V.; Han, G. W.; Jacobson, K. A.; Gao, Z. G.; Cherezov, V.; Stevens, R. C. Structure of an Agonist-Bound Human A2A Adenosine Receptor. *Science* **2011**, *332* (6027), 322−327.
(61) Liu, W.; et al. Structural Basis for Allosteric Regulation of GPCRs by Sodium Ions. *Science* **2012**, *337*, 232−236.
(62) Thompson, A. A.; et al. GPCR stabilization using the bicelle-like architecture of mixed sterol-detergent micelles. *Methods* **2011**, *55*, 310−317.
(63) Kotecha, M.; Wickramasinghe, N. P.; Ishii, Y. Efficient low-power heteronuclear decoupling in13C high-resolution solid-state NMR under fast magic angle spinning. *Magn. Reson. Chem.* **2007**, *45*, S221−S230.
(64) Lewandowski, J. R.; et al. Proton assisted recoupling at high spinning frequencies. *J. Phys. Chem. B* **2009**, *113*, 9062−9069.
(65) Thurber, K. R.; Tycko, R. Measurement of sample temperatures under magic-angle spinning from the chemical shift and spin-lattice relaxation rate of 79Br in KBr powder. *J. Magn. Reson.* **2009**, *196*, 84−87.
(66) Lee, H. J.; Lee, H. S.; Youn, T.; Byrne, B.; Chae, P. S. Impact of novel detergents on membrane protein studies. *Chem* **2022**, *8*, 980−1013.
(67) Eddy, M. T.; Yu, T.-Y.; Wagner, G.; Griffin, R. G. Structural characterization of the human membrane protein VDAC2 in lipid bilayers by MAS NMR. *J. Biomol. NMR* **2019**, *73*, 451−460.
(68) Eddy, M. T.; et al. Lipid bilayer-bound conformation of an integral membrane beta barrel protein by multidimensional MAS NMR. *J. Biomol. NMR* **2015**, *61*, 299−310.
(69) Andreas, L. B.; et al. Structure and Mechanism of the Influenza A M2 $_{18-60}$ Dimer of Dimers. *J. Am. Chem. Soc.* **2015**, *137*, 14877−14886.
(70) Porat-Dahlerbruch, G.; Struppe, J.; Quinn, C. M.; Gronenborn, A. M.; Polenova, T. 19F fast MAS (60−111 kHz) dipolar and scalar based correlation spectroscopy of organic molecules and pharmaceutical formulations. *Solid State Nucl. Magn. Reson.* **2022**, *122*, 101831.
(71) Zhu, Y.; et al. Unexpected asymmetric distribution of cholesterol and phospholipids in equilibrium model membranes. *Biophys. J.* **2024**, *123*, 3923−3934.
(72) Kučerka, N.; Nieh, M.-P.; Katsaras, J. Asymmetric Distribution of Cholesterol in Unilamellar Vesicles of Monounsaturated Phospholipids. *Langmuir* **2009**, *25*, 13522−13527.
(73) Marsh, D. Lateral Pressure Profile, Spontaneous Curvature Frustration, and the Incorporation and Conformation of Proteins in Membranes. *Biophys. J.* **2007**, *93*, 3884−3899.
(74) Cantor, R. S. Lipid Composition and the Lateral Pressure Profile in Bilayers. *Biophys. J.* **1999**, *76*, 2625−2639.
(75) Cantor, R. S. The influence of membrane lateral pressures on simple geometric models of protein conformational equilibria. *Chem. Phys. Lipids* **1999**, *101*, 45−56.
(76) Cantor, R. S. Lateral Pressures in Cell Membranes: A Mechanism for Modulation of Protein Function. *J. Phys. Chem. B* **1997**, *101*, 1723−1725.
(77) Ferré, G.; Anazia, K.; Silva, L. O.; Thakur, N.; Ray, A. P.; Eddy, M. T. Global insights into the fine tuning of human A_{2A}AR conformational dynamics in a ternary complex with an engineered G protein viewed by NMR. *Cell Reports* **2022**, *41* (12), 111844.
(78) Thakur, N.; Wei, S.; Ray, A. P.; Lamichhane, R.; Eddy, M. T. Production of human A2AAR in lipid nanodiscs for 19F-NMR and single-molecule fluorescence spectroscopy. *STAR Protoc.* **2022**, *3*, 101535.
(79) Eddy, M. T.; et al. Allosteric coupling of drug binding and intracellular signaling in the A2A adenosine receptor. *Cell* **2018**, *172*, 68−80.
(80) Schneider, C. A.; Rasband, W. S.; Eliceiri, K. W. NIH Image to ImageJ: 25 years of image analysis. *Nat. Methods* **2012**, *9*, 671−675.
(81) Wei, S.; et al. Slow conformational dynamics of the human A2A adenosine receptor are temporally ordered. *Structure* **2022**, *30*, 329−337.
(82) Cheng, Y.; Prusoff, W. H. Relationship between the inhibition constant (K1) and the concentration of inhibitor which causes 50 per cent inhibition (I50) of an enzymatic reaction. *Biochem. Pharmacol.* **1973**, *22*, 3099−3108.
(83) Bennett, A. E.; Rienstra, C. M.; Auger, M.; Lakshmi, K. V.; Griffin, R. G. Heteronuclear decoupling in rotating solids. *J. Chem. Phys.* **1995**, *103*, 6951−6958.

https://doi.org/10.1021/jacs.4c15106
J. Am. Chem. Soc. 2025, 147, 17612−17625